Biogeosciences Discuss., 9, 13987–14012, 2012
www.biogeosciences-discuss.net/9/13987/2012/
doi:10.5194/bgd-9-13987-2012

Biogeosciences Discussions

Increasing cloudiness in Arctic damps the increase in phytoplankton primary production due to sea ice receding

S. Bélanger[1], M. Babin[2], and J.-E.Tremblay[2]

[1]Université du Québec à Rimouski, Département de Biologie, Chimie et Géographie and BORÉAS, 300 allée des Ursulines, Rimouski, Québec, G5L 3A1, Canada
[2]Takuvik Joint International Laboratory (CNRS & ULaval), Département de Biologie, Québec-Océan and Arcticnet, Université Laval, Pavillon Alexandre-Vachon, 1045, av. de la Médecine, Québec (Québec), G1V 0A6, Canada

Received: 6 September – Accepted: 26 September – Published: 12 October 2012

Correspondence to: S. Bélanger (simon_belanger@uqar.ca)

Published by Copernicus Publications on behalf of the European Geosciences Union.

Abstract

The Arctic Ocean and its marginal seas are among the marine regions most affected by climate change. Here we present the results of a diagnostic model used to elucidate the main drivers of primary production (PP) trends over the 1998–2010 period at pan-Arctic and local (i.e. 9.28 km resolution) scales. Photosynthetically active radiation (PAR) above and below the sea surface was estimated using precomputed look-up tables of spectral irradiance and satellite-derived cloud optical thickness and cloud fraction parameters from the International Satellite Cloud Climatology Project (ISCCP) and sea ice concentration from passive microwaves data. A spectrally resolved PP model, designed for optically complex waters, was then used to produce maps of PP trends. Results show that incident PAR above the sea surface (PAR(0+)) has significantly decreased over the whole Arctic and sub-Arctic Seas, except over the perrennially sea ice covered waters of the Central Arctic Ocean. This fading of PAR(0+) (+8 % decade^{-1}) was caused by increasing cloudiness May and June. Meanwhile PAR penetrating the ocean (PAR(0-)) increased only along the sea ice margin over the large Arctic continental shelf where sea ice concentration declined sharply since 1998. Overall, PAR(0-) slightly increased in the Circum Arctic (+3.4 % decade^{-1}), while it decreased when considering both Arctic and sub-Arctic Seas (–3 % decade^{-1}). We showed that rising phytoplankton biomass (i.e. chlorophyll *a*) normalized by the diffuse attenuation of photosynthetically usable radiation (PUR) by phytoplankton accounted for a larger proportion of the rise in PP than did the increase in light availability due to sea-ice loss in several sectors and particularly in perrennially and seasonally open waters. Against a general backdrop of rising productivity over Arctic shelves, significant negative trends were observed in regions known for their great biological importance such as the coastal polynyas of Northern Greenland.

BGD
9, 13987–14012, 2012

1 Introduction

The impacts of environmental changes on Arctic and Sub-Arctic marine ecosystems are already detectable from field- (Grebmeier et al., 2006; Li et al., 2009) and satellite-based measurements (Arrigo and van Dijken, 2011; Arrigo et al., 2008; Kahru et al., 2011). While the overall increase in primary productivity (PP) has been attributed to a longer growing season, due to enhanced light availability for photosynthesis (Arrigo and van Dijken, 2011; Arrigo et al., 2008), changes in environmental forcing of nutrient supply to the surface have been proposed as the main driver of PP in seasonally ice-free waters (Tremblay and Gagnon, 2009).

At high northern latitudes, photosynthetically active radiation (PAR) is known to be an important limitation for marine photosynthesis. Environmental factors affecting the amount of PAR include cloud cover and the presence of sea ice and associated snow cover, which strongly attenuate shortwave radiation. While the ice and snow cover have decreased significantly in recent decades (Comiso et al., 2008), cloud cover has increased (Eastman and Warren, 2010; Wang and Key, 2005). In fact, the shortwave radiation reaching the sea surface during summer months dropped at a mean annual rate of 0.66 $W m^{-2} yr^{-1}$ between 1982 and 1999 due to increasing cloudiness (Wang and Key, 2005). Climate models predict both a reduction in sea ice and an increase in cloud cover for the 21st century as the Arctic warms (Vavrus et al., 2010). During the open water season clouds typically cover 90 % of the sky, attenuating significantly the incoming shortwave radiation. Using satellite lidar measurements of cloud properties Palm et al. (2010) found negative correlations between cloud fraction and sea ice coverage, suggesting that increasing temperature and moisture fluxes during ice-free period favors cloud formation. They also found greater low cloud frequency and cloud optical thickness above ice-free water areas (Palm et al., 2010). Although previous studies suggested that the Arctic region will become more productive overall due to a decline in the duration and extent of sea ice (Arrigo and van Dijken, 2011; Arrigo et al., 2008), the net effect of the opposing trends in the evolution of sea ice and cloud cover on PAR, and consequently on the marine primary productivity has never been assessed.

The environmental forces that control vertical mixing in the upper ocean (e.g. wind, freshwater input) and, consequently, the supply of nutrients to the sea surface, may counteract (increase stratification) (Li et al., 2009) or amplify (increased frequency of upwelling events that brings nutrient-rich waters to the surface) (Carmack and Chapman, 2003; Tremblay et al., 2011) the positive influence of increasing PAR. From the perspective of space-borne observation, a change in ocean stratification affecting nutrient supply should be detectable from the ensuing change in chlorophyll *a* concentration (CHL), a proxy for phytoplankton biomass routinely derived from remote sensing of ocean color (Behrenfeld et al., 2006).

Photosynthesis decreases when absorbing materials from terrestrial origin increase the blue light attenuation (Smyth et al., 2005). Shortly after the spring freshet, the Arctic shelves receive massive amount terrigenous colored dissolved organic matter (CDOM) and suspended particulate material (SPM). Recent studies have reported increasing coastal erosion along several arctic coastline (Rachold et al., 2000) and river runoff at northern latitudes (Peterson et al., 2006). Models also predicted an important release of DOM into the Arctic Ocean (+700 %) from the carbon-rich siberian peatlands (Frey and Smith, 2005). Diffuse light attenuation coefficient (K_d) can, therefore, change due to variations in allochtonous material input. In constrast, removal processes of optically active constituents (e.g. CDOM photobleaching) can increase light penetration and favour PP. To detect such changes from space, PP models need to consider K_d independently from CHL (e.g. Smyth et al., 2005).

The objectives of this study were (1) to assess the trends in PAR reaching the sea surface versus PAR penetrating the sea surface after considering sea ice cover, and (2) to quantify the relative contribution of changing PAR conditions due to sea ice, clouds and ocean optical properties, respectively, to the observed trends in PP. To achieve these objectives we developed a PAR model that assimilates satellite-based cloud properties and a fully spectral PP model for optically complex Arctic waters. The

BGD
9, 13987–14012, 2012

implementation of the model was initiated as part of the Malina project in order to develop long-term monitoring capabilities of the Arctic's marine ecosystems productivity. We show that, over the 1998–2010 period of ocean color observation, PAR increased only slightly (but not significantly) in Arctic waters as a result of opposing trends in cloud and sea-ice cover. Nevertheless, positive PP trends were found. They are explained by concurrent changes in PAR, CHL and K_d, and the contribution of each factor varied strongly spatially.

2 Methods

2.1 PAR model

Incident spectral downwelling irradiance just beneath the sea surface, $E_d(0-,\lambda,t)$, was computed at 5 nm resolution every 3 h using a pre-computed look-up-table (LUT) generated using Santa Barbara DISORT Atmospheric Radiative Transfer model (SBDART, Ricchiazi et al., 1998). The radiative transfer model inputs were: solar zenith angle (θ_s), total ozone concentration (O_3), cloud fraction (CF) over the pixel and cloud optical thickness (τ_{cl}). The last three parameters were derived from satellite data (mainly AVHRR; Schweiger et al. 1999) following the method developed by Zhang et al. (2004) and were obtained from the International Satellite Cloud Climatology Project (ISCCP) web site. The ISCCP global radiative flux data (FD) are distributed on a 280 km equal-area grid at 3 h intervals for dates between January 1984 and December 2009. Here, PAR(0+) refers to the integral of $E_d(\lambda)$ from 400 to 700 nm just above the sea and ice surface (in Einstein $m^{-2}\,h^{-1}$), while PAR(0−) is the is the integrated irradiance just below the sea surface after considering air-to-sea interface reflection for both direct and diffuse components of the downwelling irradiance ($\rho_{Fresnel}$) and the daily sea ice concentration (SIC; in %) (i.e. $PAR(0-) = PAR(0+)\cdot(1-\rho_{Fresnel})\cdot(1-SIC)$). Daily satellite-derived SIC data from the Defense Meteorological Satellite Program (DMSP) Scanning Multichannel Microwave Radiometer (SMMR), F8 and F13 Special Sensor Microwave Imager

BGD
9, 13987–14012, 2012
Arctic PP trends
S. Bélanger et al.

(SSMI) (1984–2007) (Cavalieri et al., 1996) and F17 Special Sensor Microwave Imager/Sounder (SSMIS) (2008–2010) sensors (Maslanik and Stroeve, 1999) were obtained from the National Snow and Ice Data Center (NSIDC).

2.2 Primary production model

Daily PP rates were calculated using a photosynthesis-irradiance model (i.e. P vs E curves):

$$\mathrm{PP} = \mathrm{CHL} \cdot \mathrm{P}_m^B \int_{t=0}^{24\,\mathrm{h}} \int_{z=0.1\,\%}^{100\,\%} 1 - e^{\frac{-\mathrm{PUR}(z,t)}{\mathrm{E}_k}} \mathrm{d}z\mathrm{d}t \tag{1}$$

chlorophyll *a* concentration (CHL; in $\mathrm{mg\,m^{-3}}$), photosynthetically usable radiation (PUR, in $\mathrm{Einstein\,m^{-2}\,s^{-1}}$), light-saturated CHL-normalized carbon fixation rate (P_m^B; in $\mathrm{mg\,C\,(mg\,CHL)^{-1}\,h^{-1}}$), and saturation irradiance (E_k, $\mathrm{Einstein\,m^{-2}\,s^{-1}}$) are needed for the calculation of PP at each depth. Ocean color data, binned at a 9.28 km resolution on a equal-area grid, were used for CHL and to calculate PUR at each depth in the water column. Briefly, monthly CHL data retrieved using a semi-analytical algorithm (GSM01) (Maritorenna et al., 2002) were obtained from the Ocean Color MEaSUREs project (v6) at UCSB http://wiki.icess.ucsb.edu/measures/Products). GSM01 was found to perform better than standard empirical algorithms (e.g. NASA's OC4v6) in Arctic waters dominated by CDOM absorption (Ben Mustapha et al., 2012). Next, SeaWiFS Level 3 monthly water-leaving reflectance ($\mathrm{R_{rs}}$) at 412, 443, 490, 510, 555 and 670 nm were obtained from the NASA GSFC (reprocessing 2010.0). Spectral IOPs, namely the total absorption (a) and backscattering (b_b) coefficients, were estimated from $\mathrm{R_{rs}}(\lambda)$ using a quasi-analytical algorithm (QAA) (Lee et al., 2002). The accuracy of the QAA in Arctic waters remains to be assess, but a preliminary validation indicated an excellent performance of this algorithm for the retrievals of the total a and b_b (absolute relative difference < 18 %) (Bélanger, 2006). The in-water spectral diffuse attenuation coefficient $K_d(\lambda)$ averaged over the euphotic zone was estimated following the approach of Lee et al. (2005) using the QAA-derived IOPs as input. $K_d(\lambda)$ was used to propagate $E_d(z,\lambda,t)$ throughout the water column. This was achieved at twelve optical depths from the sea surface to a level of 0.1 % of the incident light. $PUR(z,t)$ was calculated at each time step and depth using :

$$PUR(z,t) = \int_{\lambda=400}^{700\,nm} E^0(\lambda,z,t) \cdot \frac{a_{ph}(\lambda)}{a_{ph}(443)} d\lambda \qquad (2)$$

where $a_{ph}(\lambda)$ is the spectral phytoplankton absorption coefficient (in m^{-1}), and E^0 is the spectral scalar irradiance. The later was calculated by dividing E_d by the mean cosine of downwelling irradiance (Morel, 1991), approximated by the expression $\frac{(a+bb)}{K_d}$ (Sathyendranath et al., 1989). $a_{ph}(\lambda)$ was calculated using an empirical statistical relationship established between $a_{ph}(\lambda)$ and CHL derived from measurements made in the Western Arctic Ocean by Matsuoka et al. (2011). E_k was modeled using the Arrigo et al. (1998) model developed for high latitudes, while P_m^B was assumed to be constant at 2.0 mgC (mgCHL)$^{-1}$ h^{-1}, an averaged value based on field measurements in Arctic waters (Harrison and Platt, 1986).

PP calculations using the above model were made for each day of the year using the monthly means of the IOPs and CHL. Gaps in the monthly fields, due to presistent cloud or sea-ice cover, were filled with monthly climatology of IOPs and CHL. When OC data were available, the daily PP was computed for each day of the month. The daily PP rate of the pixel was adjusted as a function of the daily fraction of open water (1 – SIC). PP was assumed nil where no IOPs and CHL data are available (i.e. pixels never documented by SeaWiFS). This method allowed us to consider the exact same surface area from year to year for the whole time series, and thereby minimizing the possible bias introduced by the increasing number of ocean pixels documented by SeaWiFS through time as open-water area increases.

BGD
9, 13987–14012, 2012

2.3 Trends analysis

The trends in yearly PAR and PP over the 13 yr SeaWiFS time series were calculated for each pixel using a nonlinear trends estimator as described in Zhang et al. (2000). This is a non-parametric method that removes autocorrelation and outliers from the time series before calculating the trend using the Theil-Sen approach (TSA; Sen slope). The *zyp.zhang* function implemented in R was used. The Mann-Kendall non-parametric test was then run on the resulting time series to test the significance of the trends.

3 Results

3.1 Above-surface photosynthetically available radiation trends

Annual PAR reaching the sea surface (PAR(0+)) above the Arctic circle range from 3000 to 5500 Einstein $m^{-2}\,yr^{-1}$ (Fig. 1a). From 1998 to 2009, which corresponds approximately to the SeaWiFS era, PAR(0+) generally decreased at a rate raging from -100 to -50 Einstein $m^{-2}\,yr^{-1}$ over seasonally and permanently open water (Fig. 1b), while it increased ($\sim +50$ to $+100$ Einstein $m^{-2}\,yr^{-1}$) in over the permanently ice-covered Central Arctic waters. The largest decrease in PAR(0+) were found between 55° N and 70° N (Hudson Bay, Gulf of Alaska, Bering Sea and Nordic Seas). The relative changes generally lied between $\pm 2\,\%\,yr^{-1}$ (Fig. 1c). Monthly maps of PAR(0+) trends indicate that changes occurred mostly in June, May and July, respectively, depending on regions (Fig. S1, Supplement). If integrated over the whole circum Arctic waters ($\geq 66.58°$ N), PAR(0+) has decreased by $\sim 10\,\%$ over the SeaWiFS era (yellow bars on Fig. 3a). PAR(0+) tended to decrease at all summer months with the largest relative rate occurring in June ($-1.4\,\%\,yr^{-1}$) when solar irradiance is maximum (Fig. 3a).

BGD
9, 13987–14012, 2012

3.2 Below-surface photosynthetically available radiation trends

In the seasonally and permanently open water, sea ice is the primarily factor controlling the penetration of PAR in the ocean (Fig. 2a) (Perovich et al., 2007). As expected, PAR(0−) has increased significantly since 1998 at rates reaching up to +150 Einstein $m^{-2} yr^{-1}$) at the margin of the Central ice pack (Fig. 2b) resulting in a relative increase of 0.34 % yr^{-1} in PAR for the circum-Arctic waters (red bars on Fig. 3a). Interestingly, the increase in the high Arctic (≥ 70° N) was largely counter-balanced by a general decrease in PAR(0−) between 55 to 65° N (Fig. 2b). Integrating total PAR(0−) over Arctic and sub-Arctic Seas (including Okhotsk, Bering, Labrador, White Seas and Hudson complex; see Fig. S1) resulted in slightly negative trend of −0.30 % yr^{-1} (Fig. 3b).

3.3 Total circum-Arctic primary production

The PAR model was used to drive the primary production model as detailed in Sect. 2.2. Total circum-Arctic estimate of primary production was more than two fold smaller (203 ± 15 TgC yr^{-1}) than previous satellite-based estimates (i.e. 441 to 585 TgC yr^{-1}) (Arrigo et al., 2008; Arrigo and van Dijken, 2011). This departure arises partly from the choices of ocean color algorithms and photosynthetic parameters used in the model. Our PP model explicitly accounts for the fact that Arctic waters are optically complex (Matsuoka et al., 2007; Siegel et al., 2005; Bélanger et al., 2008). Firstly, total light absorption and scattering coefficients of seawater constituents were assessed from ocean color reflectance measurements to estimate the diffuse attenuation (Lee et al., 2002, 2005). Secondly, CHL was retrieved using a semi-analytical approach that minimize the effect of colored detrital mater (CDM), which is dominant in the Arctic (Bélanger et al., 2008; Matsuoka et al., 2007, 2011; Wang et al., 2005). The most important factor explaining the lower PP estimation is the lower CHL values obtained using semi-analytical model as compared to CHL empirically derived from NASA standard algorithms such as OC4v4 (Ben Mustapha et al., 2012). In addition, our PP model

BGD
9, 13987–14012, 2012

employs the spectral diffuse attenuation coefficient (K_d), estimated using a QAA (Lee et al., 2002, 2005), rather than the relationships between CHL and IOPs, and between IOPs and K_d, as usually employed in PP models developed for clear case 1 waters. Interestingly, when PP is calculated using OC4v4 CHL estimation and the Kd parameterization employed by previous studies, the total PP rises by ∼ 85 % to 357 ± 15 TgC yr^{-1}. This value is still lower than previous estimation of Arrigo et al. (2008) probably because our model does not provide PP sectors that have never been documented by SeaWiFS. Finally, the light-saturated CHL-normalized carbon fixation rate, P_m^B, which usually varies as a function of sea surface temperature in PP models, is fixed to a constant in our model (2.0 mgC $(mgCHL)^{-1}$ h^{-1}) due to a lack of robust parameterization for arctic waters.

3.4 Primary production trends

Figure 4b shows that changes are spatially heterogeneous and relatively small over most of the circum Arctic Ocean (≤ 3 gC m^{-2} yr^{-1}). The overall positive trend in PP is mostly driven by the historically productive regions of inflow (Barents and Chukchi) and interior (e.g. Kara, Laptev, East Siberian and Beaufort Seas) shelves (Fig. 4b). Because small relative changes in these productive areas can dwarf large relative changes in unproductive areas, the standardized trends presented in Fig. 4c provide a better assessment of intra-regional changes than do absolute trends. After standardization, positive trends are found on seasonally ice-free inflow and interior shelves, as well as in permanently open waters (Southern Iceland Shelf, Western Bering Sea). Negative trends are found along major exit routes of Arctic water over outflow shelves in the Eastern Greenland Sea and Canadian Archipelago (e.g. Northwestern Baffin Bay, Lancaster Sound), and in the northern part of the Bering Sea.

PP increased for each summer months (black bars in Fig. 3a). The largest increase in PP occurred during the month of May (+0.85 TgC yr^{-1} or +2.36 % yr^{-1}) followed by June (+0.65 TgC yr^{-1} or +1.54 % yr^{-1}) (Fig. 3a). A similar seasonal pattern in PP

Discussion Paper | Discussion Paper | Discussion Paper | Discussion Paper |

BGD

9, 13987–14012, 2012

Arctic PP trends

S. Bélanger et al.

trends, though with smaller relative changes ($\sim +1\,\%\,\mathrm{yr}^{-1}$), was found when considering both Arctic and sub-Arctic Seas (Fig. 3b).

3.5 Trends in ocean optical properties

The above results show that changes in PAR(0−) alone cannot explain the general increase in PP (Fig. 2 versus Fig. 4). We therefore examined whether changes in ocean optical properties can be detected and if they explain PP trends. We first calculated the trends in monthly chlorophyll *a* concentration since it is arguably the most important parameter driving the PP estimation. We found modest positive CHL trends in May and June when the increased in PP was highest ($< +0.5\,\%\,\mathrm{yr}^{-1}$), and even negative trends during the productive months of July and August ($< -0.3\,\%\,\mathrm{yr}^{-1}$) (black versus green bars in Fig. 3a). The increase in CHL, however, was more important when considering both Arctic and sub-Arctic Seas, with standardized trends reaching $1\,\%\,\mathrm{yr}^{-1}$ in June (Fig. 3b).

Our model uses satellite-derived spectral diffuse attenuation ($K_d(\lambda)$) to propagate PUR through the water column. The diffuse attenuation of PUR, K_{PUR}, which integrates the spectral effect of light avalailability for photosynthesis, is thus an appropriate quantity to examine the impact of spectral diffuse attenutation trends on PP. Because PP in Eq. (1) is proportional to CHL and inveresly proportional to K_{PUR} (i.e. $\frac{1}{K_{PUR}}$), the ratio CHL/K_{PUR} is strongly correlated to PP. In essence, this ratio expresses the the phytoplankton biomass, CHL, relative to the total diffuse attenuation background. The later varies when CDOM, SPM or phytoplankton pigments characteristics (e.g. pigment packaging) and concentration vary. In the context of a PP trends analysis, trends in ocean optical properties is best represented by CHL/K_{PUR}.

The seasonal variation in CHL/K_{PUR} is shown on Fig. 5a–d, where a general decrease is observed from May to August. Most Arctic waters exhibited very low CHL/K_{PUR} ($< 2\,\mathrm{mg\,CHL\,m^{-2}}$) relative to the North Atlantic and North Pacific. In May relatively high values were found in sectors known to host instense spring phytoplankton blooms, such as Baffin Bay and the Barents and Chukchi Seas (Fig. 5a). In contrast, CHL/K_{PUR} remained low during the whole summer season in strongly stratified arctic waters (e.g. the Canada Basin). In August, most arctic waters are strongly stratified except in regions where deep-water upwellings are dominant (e.g. NOW polynya, Northeast Greenland, Hudson Strait, Siberian coastal waters) (Fig. 5d).

The monthly trends depicted in Fig. 5e–l, showed a general increase in CHL/K_{PUR} in May, particularly in the Southern Labrador Sea. In June, the positive trends are found in the Northern Labrador, Barents and Bering Seas (Fig. 5f, j). In July, positive trends are found in Hudson Bay, arround Southern Greenland and in the Southern Barents and Chukchi Seas (Fig. 5g, k), whereas relatively strong negative trends occurred in coastal waters of Northern Greenland. When CHL/K_{PUR} increases, the phytoplankton biomass increases relative to light attenuation, thus resulting in higher PP. Therefore, as for PP, we observed an overall increase in CHL/K_{PUR} for all months in both the circum Arctic and the combined Arctic and sub-Arctic Seas (Figs. 3 and 5e–l).

4 Discussion and conclusions

The decrease in PAR(0+) over open water was nearly ubiquitous between 55° N and 70° N, with decadal reduction of 8 % for the integrated Arctic and sub-Arctic Seas and up to 20 % in specific areas. This trend is consistent with several studies reporting strong positive anomalies in cloud amount above newly opened waters during summer and early fall (Eastman and Warren, 2010; Vavrus et al., 2010; Palm et al., 2010; Wang and Key, 2005). Increased cloudiness thus partly counteracts the positive influence of declining sea ice on PAR(0−) and renders the change in PAR(0−) non significant over the 13-yr study period (+3.4 % per decade in the circum Arctic and −3 % over both Arctic and sub-Arctic Seas; Fig. 3). Warmer temperature and moisture fluxes are likely the main drivers of the increase in cloudiness (Eastman and Warren, 2010; Vavrus et al., 2010; Palm et al., 2010; Wang and Key, 2005). The positive trends over the perennally ice-covered ocean is, however, more uncertain due to the lower quality of cloud

BGD
9, 13987–14012, 2012

properties retrievals over ice covered conditions (Schweiger et al., 1999; Chernokulsky and Mokhov, 2012).

Previous analyses of satellite-based PP time series revealed significant variability in spatial patterns and temporal trends across Arctic marine ecosystems (Arrigo and van Dijken, 2011; Arrigo et al., 2008; Kahru et al., 2011; Perrette et al., 2011). Here we also found a significant ($p < 0.05$) PP trend of +2.8 TgC yr^{-1} (or +1.4 % yr^{-1} in relative terms; Fig. 3a) between 1998 and 2010 for the circum-Arctic. Longer growing season and light availability (i.e. PAR(0−)) was previously identified as a main driver of change in the high Arctic (Arrigo and van Dijken, 2011; Arrigo et al., 2008). We also found a correlation between annual PAR and PP anomalies across the circum-Arctic ($r^2 = 0.42$, $p < 0.001$; not shown). However, changes in light availability do not alone explain the positive PP trends in many Arctic sectors, except on Arctic interior shelves where PAR(0−) is largely driven by SIC (Figs. 2 versus 4). In many regions, such as Hudson Bay, Baffin Strait, Baffin Bay and the Labrador, Norwegian and Barents Seas, PAR(0−) decreased while PP increased. The pattern in Fig. 5 shows that this observation can only be explained by a change in ocean optical properties, here expressed as the ratio of chlorophyll *a* concentration to the diffuse attenuation coefficient of photosynthetically usable radiation (CHL/K_{PUR}) (Fig. 5). This ratio seems to provide a good proxy for trophic state of Arctic and Sub-Arctic waters.

In general, low CHL/K_{PUR} values occurred in stratified, nutrients-depleted surface waters, while high values were found in productive waters sustained by nutrients inputs from rivers or the deep ocean (Fig. 5a–d). In several Arctic sectors, for example, the haline stratification limits nutrient supply, explaining the low surface CHL. In these waters, however, the diffuse attenuation remained relatively important due to the high background in colored detrital materials (CDM). The high CDM background in the Arctic polar mixed layer (PML) is due to the relatively high concentration of CDOM from both terrestrial and marine origin (Stedmon et al., 2011). In the Barents Sea in summer, low CHL/K_{PUR} ratio resulting from concurent low surface CHL and high CDM background (Fig. 5b–d) could be due to the in situ production of CDOM during the consumption of the spring bloom that occured in May (Fig. 5a). Indeed, CDOM production from microbial activity is often decoupled from phytoplankton production and is delay after the spring bloom (Nelson et al., 1998). In sectors where river inputs are dominant, however, very high values of CHL/K_{PUR} may be overestimated due to the difficulty to distinguish CHL from other optically active constituents. Improvements of ocean color algorithms for both CHL and K_d remains a major issue in the coastal arctic (Ben Mustapha et al., 2012).

CHL/K_{PUR} remained relatively constant within Arctic interior shelves, possibly because sea ice and clouds limit the number of good quality data in these environments. The general rise in CHL/K_{PUR} observed in permanently open waters during May could be related to increasingly early stabilization of the water column in spring, resulting in earlier phytoplankton blooms (Kahru et al., 2011). The positive PP trends in the Labrador Sea (Fig. 4), for example, are due to increasing values in CHL/K_{PUR} from south to north in early summer (Fig. 5i, j). Similarly, high PP in the Barents Sea is mostly driven by the strong positive trend in CHL/K_{PUR} in June and July (Fig. 5j, k).

Despite a general positive trend in PP over much of the Arctic, we found strong indications that PP is declining in regions of prime ecological importance. Negative PP trends were mostly explained by a reduction of PAR due to increasing cloudiness (Fig. 1) in the Northern Bering Sea (Fig. 4) and by higher SIC and lower penetration of sun light in the water column (Fig. 2) near the location of the northeast water (NEW) polynya. The latter result may be due to an increase in sea-ice export trough Fram Strait since 2003 as reported recently by Kwok et al. (2009). The North Water (NOW) polynya, located in the Northern Baffin Bay, experienced one of the most severe drop in PP ($5\,gC\,m^{-2}\,yr^{-1}$; Fig. 4b). With an area of $80\,000\,km^2$, the NOW has been considered to be the most productive recurrent polynya north of 77° N due to a long and intense diatom bloom that starts in May and fuels a rich marine ecosystem supporting polar cod, large aggregations of marine mammals, sea birds and polar bears (Tremblay et al., 2006). Our results indicate that the timing of this bloom may have changed over time. Indeed, a modest increase in CHL/K_{PUR} in May was followed by a sustained decrease

BGD
9, 13987–14012, 2012

in June and July (Fig. 5), which was primarily responsible for the decline in the annual productivity of the NOW. These results raise questions about the ultimate drivers of changes in the NOW. We speculate that bloom dynamics are linked to changes in the quantity or properties (e.g. salinity, nutrients, CDOM) of the in-flow of cold, nutrient-depleted waters coming from the Arctic Ocean (Kwok et al., 2010; Münchow et al., 2011).

Another limitations are inherent to our satellite-based PP trends assessment. First, our method cannot detect if changes occured in the subsurface chlorophyll *a* maximum (SCM), which can be important in the Arctic waters during the summer period (Martin et al., 2012). Recent studies, however, suggested that the error in the annual PP assessment resulting from the omission of the SCM is small, but more important during the post-bloom period in late summer (Ardyna et al., 2012; Arrigo and van Dijken, 2011). Second, under-ice phytoplankton blooms, which are undetectable from space, may be more important than previously thought. These blooms have been observed in different Arctic sectors and can locally represent most of the annual PP (Arrigo et al., 2012; Mundy et al., 2009).

High spatial resolution maps of PP trends, together with those in PAR(0+), PAR(0−) and CHL/K_{PUR}, provide new insights about the main drivers of changes in primary productivity across the Arctic and Sub-Arctic marine ecosystems. Future developpements of long-term monitoring capabilities of marine arctic ecosystems should, among other, (1) include improvements in the ocean color algorithms to reduce the uncertainty on the satellite-based PP estimation in optically complex waters, (2) address the problem of data continuity to produce consistent time series of ocean color and other sensors, (3) evaluate and compare methods used to estimate PAR reaching the sea surface under cloud and ice conditions and (4) examine in more details the environmental variability (e.g. SST, wind speed, storms frequency, etc.) to better understand the most important drivers of changes in the ocean optical properties and PP.

BGD
9, 13987–14012, 2012

Supplementary material related to this article is available online at: http://www.biogeosciences-discuss.net/9/13987/2012/ bgd-9-13987-2012-supplement.pdf.

Acknowledgements. This work was supported by a NSERC discovery grant to S.B. and a WWF-Canada contract to Arctus inc. The authors are grateful to James Snider and Peter Ewins (WWF-Canada) and Servet Cizmeli and Laurens Put (Arctus inc.) for their contributions to the study. They also acknowledge the NASA Ocean Color team for providing SeaWiFS data and S. Maritorena for access to GSM data, as well as X. Zhang from the ISCCP project for provision of the surface fluxes data products. This is a contribution to the ArcticNet and Manila programs.

References

Ardyna, M., Babin, M., Gosselin, M., Devred, E., Bélanger, S., and Matsuoka, A.: Parameterization of the vertical chlorophyll *a* in the Arctic Ocean: impact of subsurface chlorophyll maximum to regional annual ans seasonal primary production estimates, Biogeosciences Discuss., in preperation, 2012. 14001

Arrigo, K. R. and van Dijken, G. L.: Secular trends in Arctic Ocean net primary production, J. Geophys. Res., 116, C09011, doi:10.1029/2011JC007151, 2011. 13989, 13995, 13999, 14001

Arrigo, K. R., Worthen, D., Schnell, A., and Lizotte, M. P.: Primary production in Southern Ocean waters, J. Geophys. Res., 103, 15587–15600, 1998. 13993

Arrigo, K. R., van Dijken, G., and Pabi, S.: Impact of a shrinking Arctic ice cover on marine primary production, Geophys. Res. Lett., 35, L19603, doi:10.1029/2008GL035028, 2008. 13989, 13995, 13996, 13999

Arrigo, K. R., Matrai, P. A., and van Dijken, G. L.: Primary productivity in the Arctic Ocean: impacts of complex optical properties and subsurface chlorophyll maxima on large-scale estimates, J. Geophys. Res., 116, C110022, doi:10.1029/2011JC007273, 2011.

Arrigo, K. R., Perovich, D. K., Pickart, R. S., Brown, Z. W., van Dijken, G. L., Lowry, K. E., Mills, M. M., Palmer, M. A., Balch, W. M., Bahr, F., Bates, N. R., Benitez-Nelson, C., Bowler, B., Brownlee, E., Ehn, J. K., Frey, K. E., Garley, R., Laney, S. R., Lubelczyk, L., Mathis, J., Matsuoka, A., Mitchell, B. G., Moore, G. W. K. , Ortega-Retuerta, E., Pal, S., Polashenski, C. M., Reynolds, R. A., Schieber, B., Sosik, H. M., Stephens, M., and Swift, J. H.: Massive Phytoplankton Blooms Under Arctic Sea Ice, Science, 336, 1408, doi:10.1126/science.1215065, 2012. 14001

Behrenfeld, M. J., Malley, R. T. O., Siegel, D. A., Mcclain, C. R., Sarmiento, J. L., Feldman, G. C., Milligan, A. J., Falkowski, P. G., Letelier, R. M., and Boss, E. S.: Climate-driven trends in contemporary ocean productivity, Nature, 444, 752–755, doi:10.1038/nature05317, 2006. 13990

Ben Mustapha, S., Larouche, P., and Bélanger, S.: Evaluation of ocean color algorithms in the Southeastern Beaufort Sea: new parameterization using SeaWiFS, MODIS and MERIS spectral bands, Can. J. Remote Sensing, in press, 2012. 13992, 13995, 14000

Bélanger, S.: Response of light-related carbon fluxes in the Arctic Ocean to climate change: quantification and monitoring of dissolved organis matter photo-oxidation in the Beaufort Sea using satellite remote sensing, PhD thesis, Université Pierre et Marie Curie, Paris, France, 243 pp., 2006. 13992

Bélanger, S., Babin, M., and Larouche, P.: An empirical ocean color algorithm for estimating the contribution of chromophoric dissolved organic matter to total light absorption in optically complex waters, J. Geophys. Res., 113, C04027, doi:10.1029/2007JC004436, 2008. 13995

Carmack, E. C. and Chapman, D. C.: Wind-driven shelf/basin exchange on an Arctic shelf: the joint roles of ice cover extent and shelf-break bathymetry, Geophys. Res. Lett., 30, 1778, doi:10.1029/2003GL017526, 2003. 13990

Cavalieri, D. J., Parkinson, C., Gloersen, P., and Zwally, H. J.: Sea Ice Concentrations from Nimbus-7 SMMR and DMSP SSM/I Passive Microwave Data, (1998–2007), 1996. 13992

Chernokulsky, A. and Mokhov, I. I.: Climatology of total cloudiness in the Arctic: an intercomparison of observations and reanalyses, Adv. Meteoro., 2012, 1–15, doi:10.1155/2012/542093, 2012. 13999

Comiso, J. C., Parkinson, C. L., Gersten, R., and Stock, L.: Accelerated decline in the Arctic sea ice cover, Geophys. Res. Lett., 35, 1–6, doi:10.1029/2007GL031972, 2008. 13989

Eastman, R. and Warren, S. G.: Interannual variations of Arctic cloud types in relation to sea ice, J. Climate, 23, 4216–4232, doi:10.1175/2010JCLI3492.1, 2010. 13989, 13998

Frey, K. E. and Smith, L. C.: Amplified carbon release from vast West Siberian peatlands by 2100, Geophys. Res. Lett., 32, L09401, doi:10.1029/2004GL022025, 2005. 13990

BGD
9, 13987–14012, 2012

Arctic PP trends

S. Bélanger et al.

Grebmeier, J. M., Overland, J. E., Moore, S. E., Farley, E. V., Carmack, E. C., Cooper, L. W., Frey, K. E., Helle, J. H., McLaughlin, F. A., and McNutt, S. L.: A major ecosystem shift in the Northern Bering Sea, Science, 311, 1461–1464, 2006. 13989

Harrison, W. G. and Platt, T.: Photosynthesis-irradiance relationships in polar and temperate phytoplankton populations, Polar Biol., 5, 153–164, 1986. 13993

Kahru, M., Brotas, V., Manzano-Sarabia, M., and Mitchell, B. G.: Are phytoplankton blooms occurring earlier in the Arctic?, Glob. Change Biol., 17, 1733–1739, doi:10.1111/j.1365-2486.2010.02312.x, 2011. 13989, 13999, 14000

Kwok, R., Cunningham, G. F., Wensnahan, M., Rigor, I., Zwally, H. J., and Yi, D.: Thinning and volume loss of the Arctic Ocean sea ice cover: 2003–2008, J. Geophys. Res., 114, C07005, doi:10.1029/2009JC005312, 2009. 14000

Kwok, R., Toudal Pedersen, L., Gudmandsen, P., and Pang, S. S.: Large sea ice outflow into the Nares Strait in 2007, Geophys. Res. Lett., 37, L03502, doi:10.1029/2009GL041872, 2010. 14001

Lee, Z.-P., Carder, K. L., and Arnone, R. A.: Deriving inherent optical properties from water color: a multiband quasi-analytical algorithm for optically deep waters, App. Opt., 41, 5755–5772, 2002. 13992, 13995, 13996

Lee, Z. P., Du, K. P., and Arnone, R.: A model for the diffuse attenuation coefficient of downwelling irradiance, J. Geophys. Res., 110, C02016, doi:10.1029/2004JC002275, 2005. 13993, 13995, 13996

Li, W. K. W., McLaughlin, F. A., Lovejoy, C., and Carmack, E. C.: Smallest algae thrive as the Arctic Ocean freshens, Science, 326, 539, doi:10.1126/science.1179798, 2009. 13989, 13990

Maritorena, S., Siegel, D. A., and Peterson, A. R.: Optimization of a semianalitical ocean color model for global-scale applications, App. Opt., 41, 2705–2714, 2002. 13992

Martin, J., Tremblay, J.-E., Gagnon, J., Tremblay, G., Lapoussiere, A., Jose, C., Poulin, M., Gosselin, M., Gratton, Y., and Michel, C.: Prevalence, structure and properties of subsurface chlorophyll maxima in Canadian Arctic waters, Mar. Ecol. Progr. Series, 412, 69–84, doi:10.3354/meps08666, 2010. 14001

Maslanik, J. A. and Stroeve, J. C.: Near-Real-Time DMSP SSM/I-SSMIS Daily Polar Gridded Sea Ice Concentrations, (2008–2010), Boulder, Colorado USA: National Snow and Ice Data Center, Digital media, 1999. 13992

BGD

9, 13987–14012, 2012

Arctic PP trends

S. Bélanger et al.

Matsuoka, A., Huot, Y., Shimada, K., Saitoh, S.-I., and Babin, M.: Bio-optical characteristics of the Western Arctic Ocean: implications for ocean color algorithms, Can. J. Remote Sens., 33, 503–518, 2007. 13995

Matsuoka, A., Hill, V., Huot, Y., Babin, M., and Bricaud, A.: Seasonal variability in the light absorption properties of Western Arctic waters: parameterization of the individual components of absorption for ocean color applications, J. Geophys. Res., 116, 1–15, doi:10.1029/2009JC005594, 2011. 13993, 13995

Morel, A.: Light and marine photosynthesis: a spectral model with geochemical and climatological implications, Prog. Oceanogr., 26, 263–306, 1991. 13993

Münchow, A., Falkner, K. K., Melling, H., Rabe, B., and Johnson, H. L.: Ocean warming and freshening of Nares Strait bottom waters off NW Greenland 2003–09, Oceanography, 24, 114–123, doi:10.5670/oceanog.2011.62, 2011. 14001

Mundy, C. J., Gosselin, M., Ehn, J., Gratton, Y., Rossnagel, A., Barber, D. G., Martin, J., Tremblay, J.-É., Palmer, M., Arrigo, K. R., Darnis, G., Fortier, L., Else, B., and Papakyriakou, T.: Contribution of under-ice primary production to an ice-edge upwelling phytoplankton bloom in the Canadian Beaufort Sea, Geophys. Res. Lett., 36, L17601, doi:10.1029/2009GL038837, 2009. 14001

Nelson, N. B., Siegel, D. A., and Michaels, A. F.: Seasonal dynamics of colored dissolved material in the Sargasso Sea, Deep-Sea Res., 45, 931–957, 1998. 14000

Palm, S. P., Strey, S. T., Spinhirne, J., and Markus, T.: Influence of Arctic sea ice extent on polar cloud fraction and vertical structure and implications for regional climate, J. Geophys. Res., 115, 1–9, doi:10.1029/2010JD013900, 2010. 13989, 13998

Perovich, D. K., Light, B., Eicken, H., Jones, K. F., Runciman, K., and Nghiem, S. V.: Increasing solar heating of the Arctic Ocean and adjacent seas, 1979–2005: attribution and role in the ice-albedo feedback, Geophys. Res. Lett., 34, L19505, doi:10.1029/2007GL031480, 2007. 13995

Perrette, M., Yool, A., Quartly, G. D., and Popova, E. E.: Near-ubiquity of ice-edge blooms in the Arctic, Biogeosciences, 8, 515–524, doi:10.5194/bg-8-515-2011, 2011. 13999

Peterson, B. J., McClelland, J. W., Curry, R., Holmes, R. M., Walsh, J. E., and Aagaard, K.: Trajectory shifts in the Arctic and Subarctic freshwater cycle, Science, 313, 1061–1066, 2006. 13990

Rachold, V., Grigoriev, M. N., Are, F. E., Solomon, S., Reimnitz, E., Kassens, H., and Antonow, M.: Coastal erosion vs riverine sediment discharge in the Arctic Shelf Seas, Int. J. Earth Sci., 89, 450–460, doi:10.1007/s005310000113, 2000. 13990

Ricchiazzi, P., Yang, S. R., Gautier, C., and Sowle, D.: SBDART: a research and teaching software tool for plane-parallell radiative transfer in the Earth atmosphere, B. Am. Meteorol. Soc., 79, 2101–2114, 1998. 13991

Sathyendranath, S., Platt, T., Caverhill, C. M., Warnock, R. E., and Lewis, M. R.: Remote sensing of oceanic primary production: computations using a spectral model, Deep-Sea Res., 36, 431–453, 1989. 13993

Schweiger, A. J., Lindsay, R. W., Key, J. R., and Francis, J. A.: Arctic clouds in multiyear satellite data sets, Geophys. Res. Lett., 26, 1845, doi:10.1029/1999GL900479, 1999. 13991, 13999

Siegel, D., Maritorena, S., Nelson, N. B., Behrenfeld, M. J., and McClain, C. R.: Colored dissolved organic matter and its influence on the satellite-based characterization of the ocean biosphere, Geophys. Res. Lett., 32, L20605, doi:10.1029/2005GL024310, 2005. 13995

Smyth, T. J., Tilstone, G. H., and Groom, S. B.: Integration of radiative transfer into satellite models of ocean primary production, J. Geophys. Res., 110, C10014, doi:10.1029/2004JC002784, 2005. 13990

Stedmon, C. A., Amon, R. M. W., Rinehart, A. J., and Walker, S. A.: The supply and characteristics of colored dissolved organic matter (CDOM) in the Arctic Ocean: pan Arctic trends and differences, Mar. Chem., 124, 108–118, doi:10.1016/j.marchem.2010.12.007, 2011. 13999

Tremblay, J.-É. and Gagnon, J.: The effects of irradiance and nutrient supply on the productivity of Arctic waters: a perspective on climate change, in: Influence of climate chang on changing Arctic and sub-arctic conditions, edited by: Nihoul, J. C. J. and Kostianoy, A. G., 73–89, Springer, 2009. 13989

Tremblay, J. E., Hattori, H., Michel, C., Ringuette, M., Mei, Z.-P., Lovejoy, C., Fortier, L., Hobson, K. A., Amiel, D., and Cochran, J. K.: Trophic structure and pathways of biogenic carbon flow in the Eastern North Water Polynya, Prog. Oceanogr., 71, 402–425, 2006. 14000

Tremblay, J.-É., Bélanger, S., Barber, D. G., Asplin, M., Martin, J., Darnis, G., Fortier, L., Gratton, Y., Link, H., Archambault, P., Sallon, A., Michel, C., Williams, W. G., Philippe, B., and Gosselin, M: Climate forcing multiplies biological productivity in the coastal Arctic Ocean, Geophys. Res. Lett., 38, L18604, doi:10.1029/2011GL048825, 2011. 13990

Vavrus, S., Holland, M. M., and Bailey, D. A.: Changes in Arctic clouds during intervals of rapid sea ice loss, Clim. Dynam., 36, 1475–1489, doi:10.1007/s00382-010-0816-0, 2010. 13989, 13998

Wang, X. and Key, J. R.: Arctic surface, cloud, and radiation properties based on the AVHRR Polar pathfinder dataset. Part II: recent trends, J. Climate, 18, 2575–2593, 2005. 13989, 13998

Wang, J., Cota, G., and Ruble, D. A.: Absorption and backscattering in the Beaufort and Chukchi Seas, J. Geophys. Res., 110, C04014, doi:10.1029/2002JC001653, 2005. 13995

Zhang, X., Vincent, L. A., Hogg, W. D., and Niitsoo, A.: Temperature and precipitation trends in Canada during the 20th Century, Atmos. Ocean, 38, 395–429, 2000. 13994

Zhang, Y. C., Rossow, W. B., Lacis, A. A., Oinas, V., and Mishchenko, M. I.: Calculation of radiative fluxes from the surface to top of atmosphere based on ISCCP and other global data sets: refinements of the radiative transfer model and the input data, J. Geophys. Res., 109, D19105, doi:10.1029/2003JD004457, 2004. 13991

BGD

9, 13987–14012, 2012

Arctic PP trends

S. Bélanger et al.

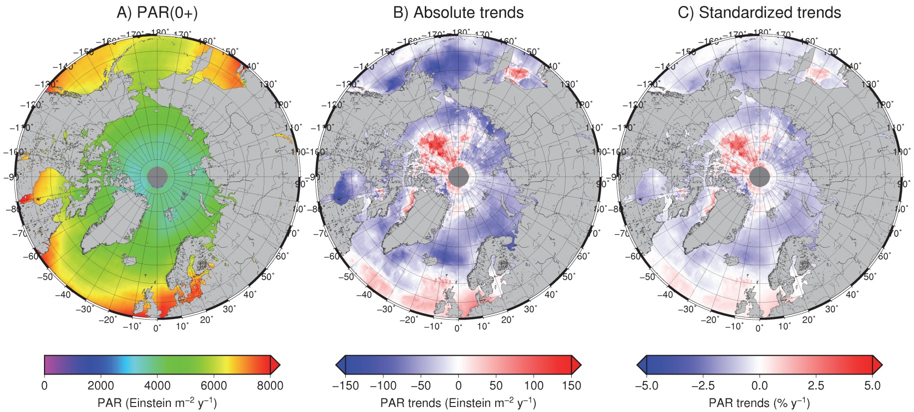

Fig. 1. (A) Mean yearly downwelling flux of PAR above de sea (ice) surface (PAR(0+)) for the 1998 to 2009 period, **(B)** Absolute PAR(0+) trends calculated using the TSA, and **(C)** the standardized PAR(0+) trends (i.e. PAR(0+) trends/climatological PAR(0+) · 100).

BGD
9, 13987–14012, 2012

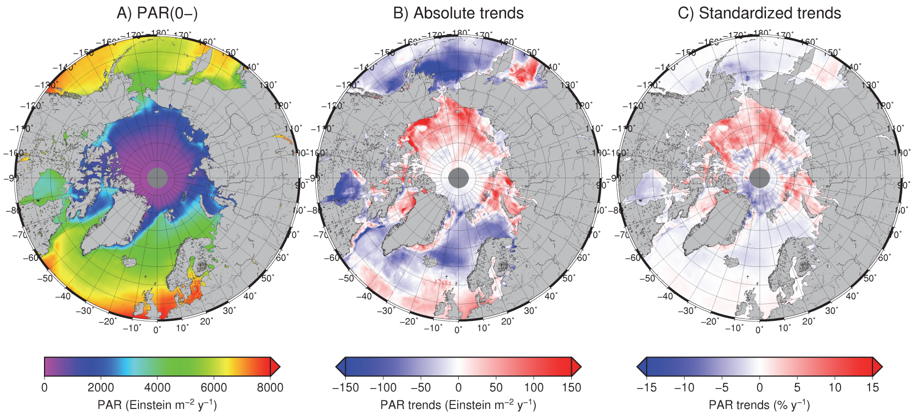

Fig. 2. Same as Fig. 1, but for PAR just below the air-sea interface (PAR(0−)).

Discussion Paper | Discussion Paper | Discussion Paper | Discussion Paper |

BGD

9, 13987–14012, 2012

Arctic PP trends

S. Bélanger et al.

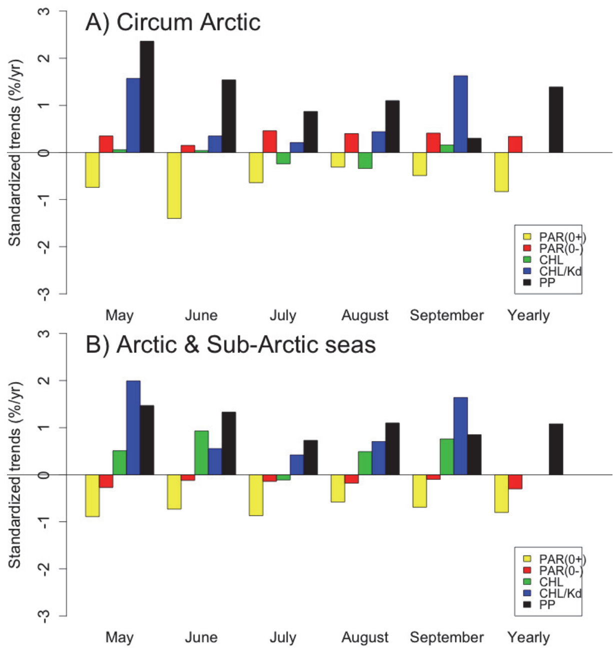

Fig. 3. (A) Monthly trends in PAR(0+), PAR(0−), CHL, CHL/K_{PUR} and PP for the circum Arctic waters (above the Arctic circle at 66.58° N). Yearly trends are only shown for PAR(0+), PAR(0−), and PP. **(B)** same as **(A)**, but for all regions considered as Arctic and Sub-Arctic seas, which include region below the Arctic circles infested by sea ice or melt glacier for at least on part of the year (e.g. Hudson Bay, Labrador Sea, Gulf of Alaska) (See Fig. S1 for the exact limits of the seas defined by the International Hydrographic Organization).

BGD
9, 13987–14012, 2012

Arctic PP trends

S. Bélanger et al.

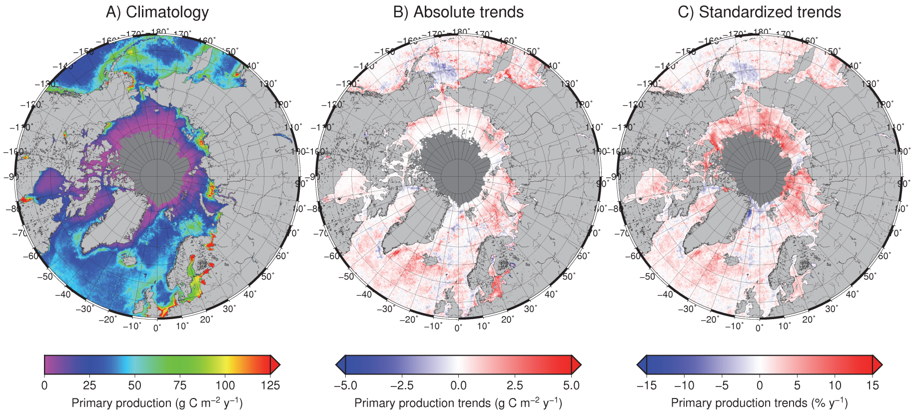

Fig. 4. (A) Climatological primary production rates for the 13 yr SeaWiFS time series (1998–2010), **(B)** Absolute PP trends calculated using the TSA, and **(C)** the standardized PP trends (i.e. PP trends/climatological PP · 100).

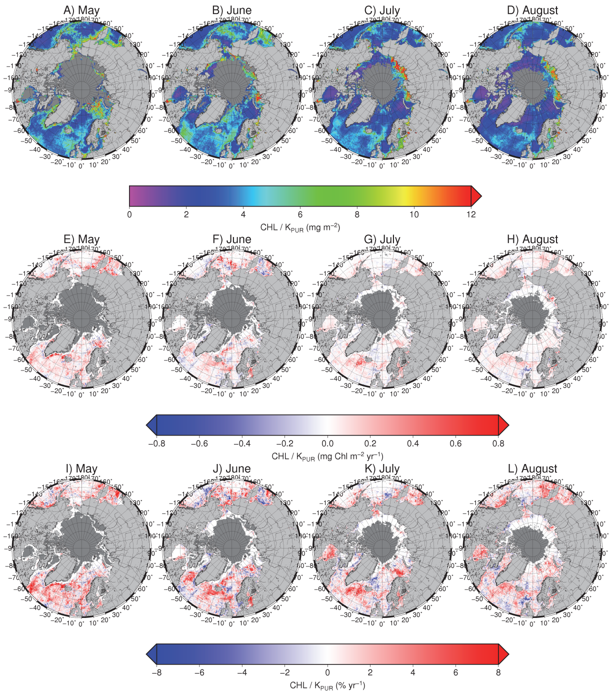

Fig. 5. (A–D) Monthly climatology of the ratio between CHL and the diffuse attenuation of PUR (CHL/K_{PUR}); **(E–H)** absolute CHL/K_{PUR} trends calculated using the TSA, and **(I–L)** the standardized CHL/K_{PUR} trends (i.e. CHL/K_{PUR} trends/climatological $CHL/K_{PUR} \cdot 100$).

Discussion Paper | Discussion Paper | Discussion Paper | Discussion Paper |

BGD

9, 13987–14012, 2012

Arctic PP trends

S. Bélanger et al.